Journal of Flow Visualization & Image Processing, vol. 9, pp. 193–210, 2002

REVERSE FLOW PHENOMENON IN A ROTATING DIFFUSER

Brane Širok, Tom Bajcar and Matevz Dular
Faculty of Mechanical Engineering, University of Ljubljana, Askerceva 6, P.O. Box 394, SI - 1000 Ljubljana, Slovenia

A study of the reverse flow phenomenon at the outlet of a rotating axial diffuser with a circular cross-section is presented in the paper. Measurement of the flow velocity components was performed by the LDA system. In addition, computer-aided visualization of the flow structures was carried out. The results showed a certain dependence of the position and size of the recirculation zone in the diffuser outlet transverse section on the amount of airflow and on the rotating frequency of the diffuser. The computer-aided visualization method proved to be more suitable for detecting the position and shape of the reverse flow regions.

INTRODUCTION

The main problem of diffusers in general is connected with their divergence angle. Large diffuser divergence angles (>14°) cause separation of the boundary layer, which in turn deteriorates the diffuser efficiency [1, 2]. On the other hand, diffusers with small divergence angles have to be very long to provide a sufficient pressure rise, however, at rather high friction losses.

Axial pressure gradient $\partial p/\partial x$ is one of the most important factors that influence the flow inside a stationary diffuser. When the axial pressure gradient is streamwise positive (which is always the case with diffusers), it causes the boundary layer at the diffuser wall to thicken and eventually (at sufficiently large diffuser divergence angles) to separate from the wall. The result is the reverse flow, which reduces the diffuser's effective transverse section area and, thus, pressure recovery.

Swirl flows, which appear in rotating diffusers as well as in axially rotating pipes [3, 4], are affected by the radial pressure gradient as well. This is the consequence of the centrifugal force caused by the rotating fluid inside the diffuser. The radial pressure gradient in its simplest form can be expressed as [5]:

$$\frac{\partial p}{\partial r} = \rho \cdot \frac{u_t^2}{r} \tag{1}$$

*Address all correspondence to Prof. Brane Širok. brane.sirok@fs.uni-lj.si.

NOMENCLATURE

A_c	average grey level in a window cell
d_i	diffuser inlet diameter (mm)
d_o	diffuser outlet diameter (mm)
d_{xc}, d_{yc}	dimensions (= number of pixels) of a window cell
E_p	grey intensity of the observed pixel
f	rotating frequency (Hz)
f_s	frequency of collecting the sequence of images (s^{-1})
i	number of cell columns in a window
i_p, j_p	co-ordinates of relative position of pixel within cell location
i_m, j_m	co-ordinates of the cell with maximum grey-level gradient
j	number of cell rows in a window
L	length of the conical part of the diffuser (mm)
n	consecutive number of an image in a sequence
N	number of all images in the sequence
p	static pressure, ($kgm^{-1}s^{-2}$)
Re_i	inlet Reynolds number
r	radius (m)
u_t	tangential velocity component (ms^{-1})
$\dot{V}$	volumetric airflow (m^3s^{-1})
x, y	Cartesian co-ordinates (mm)

Greek symbols

μ	mean value of the grey intensity in a cell for a whole sequence of images
θ	diffuser divergence angle (^{o})
ρ	density (kgm^{-3})

Equation 1 shows the equilibrium between the radial pressure gradient (left side of the equation) and the centrifugal force (right side of the equation). When the radial pressure gradient is sufficiently high, a region of low pressure is formed near the longitudinal axis of the rotating diffuser, and the fluid downstream of the diffuser outlet is sucked back towards the diffuser. Thus the flow is leaving the diffuser in the near-wall region only, since there is a large zone of reverse flow near the longi-

tudinal axis of the diffuser (the so-called "central toroidal recirculation zone" — CTRZ). This phenomenon is known as "vortex breakdown" [6–9].

Both reverse flows, the one caused by the axial pressure gradient and the one caused by the radial pressure gradient, are usually non-stationary phenomena. Therefore, it is often hard to determine the exact boundary between the main flow and the reverse flow in the diffuser transverse section. This boundary represents the line where the axial velocity component of fluid flow is actually zero (i.e. boundary line or zero axial velocity line). There exist several different methods for measuring velocity components of the flow; one of the best known measuring methods which do not disturb the flow is the LDA system. The main problem of this method for finding the zero axial velocity line is that the LDA system only measures velocity components in one point at a time. The position of the boundary between the main flow and the reverse flow may change with time because of the non-stationary character of the reverse flow. Thus it is virtually impossible to determine the exact position of the whole boundary line at the same time as one point of the boundary is found, for the position of the previously found points of zero axial velocity may already have changed. In addition, the velocities of several particles of pollutant in one measuring point are averaged by the LDA system. Thus the mean values of the measured particle velocities are quite small (e.g., close to zero) in the vicinity of the boundary line, but the standard deviation around the mean value can be high. Apart from that, a small number of particles having velocities slightly above (or below) zero can drastically change the whole measurement. The result of all this is an unclear boundary between the main flow and the reverse flow. Instead, a time-averaged region of the reverse flow is obtained.

The visualization method can be used as an alternative for determination of the zero axial velocity line. One of the most important aspects of this method is that the whole reverse flow region can be observed at once, including the sharp boundary between the two flows. Furthermore, the time-averaged region of the reverse flow can also be found by the method of computer-aided visualization and by using the maximum gradient method.

Both aforementioned methods were applied on an experimental axial diffuser with the divergence angle of 18°. The diffuser could rotate around its longitudinal axis, so both types of reverse flow could be encountered and observed. The results of both methods were compared and thoroughly discussed.

LAYOUT OF THE EXPERIMENT

The experimental station shown in Fig. 1 was used for the comparison of the LDA and visualization methods for finding the reverse flow region in the outlet transverse section of the diffuser.

A rotating conical diffuser was made of plexiglas and fastened through a steel outer pipe connection and bearings to a non-rotating inner pipe. The length L of the conical part of the diffuser was 165 mm with the inner divergence angle $\theta = 18^{\circ}$. The diffuser inlet (d_i) and outlet (d_o) diameters were 60 mm and 112.27 mm, respectively. The diffuser rotated around its longitudinal axis and was driven by an electric motor. An ejector was used as a particle generator which provided passive pollutant (droplets of water mixed with glycol) to the airflow for LDA measurements, and was located at the end of the non-rotating pipe (Fig. 1). The same ejector was used for flow visualization as well. Ejection of droplets was carried out by pressurized air at 4 bar, and a separate axial airflow of 4 l/s entered the non-rotating pipe through the particle generator. Axial airflow through the diffuser could be increased by introducing additional airflow to the non-rotating pipe from a controlled fan. Integral axial airflows up to 13.8 l/s could therefore be achieved in the diffuser. The flow of the passive pollutant was negligible compared to the airflow in the diffuser.

Three different diffuser airflows were selected for the experiments: $\dot{V} = 4$ l/s, $\dot{V} = 8$ l/s and $\dot{V} = 13.8$ l/s, with the appropriate axial inlet Reynolds numbers $\mathrm{Re}_i = 5.84 \cdot 10^3$, $\mathrm{Re}_i = 1.17 \cdot 10^4$, and $\mathrm{Re}_i = 2.01 \cdot 10^4$, respectively. The diffuser was either stationary or rotating at a rotating frequency $f = 52.8$ Hz. Combination of the se-

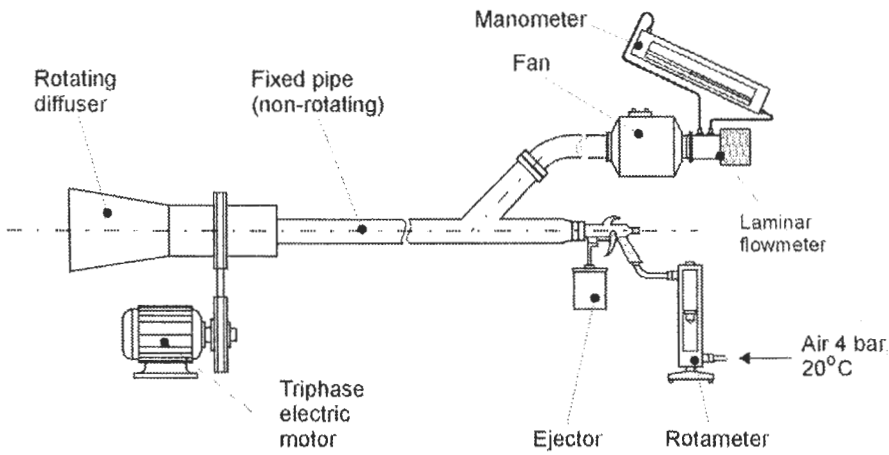

Fig. 1 Schematic diagram of the experimental station.

lected airflows and rotating frequencies resulted in 6 different operating conditions of the diffuser, at which the reverse flow phenomenon was observed.

Measurements of the axial velocity components at the diffuser outlet were performed by a TSI two-component, back-scatter LDA system with a Spectra Physics Model 2016 argon-ion laser. The LDA system incorporated two TSI Model 9180A frequency shifters to make directional sensitivity possible. A TSI Model 9275-1 fibre optical probe was mounted on a three-axis traversing system with the resolution smaller than 0.01 mm. The system also incorporated two IFA 550 flow analysers, one for each component.

Axial velocity component measurements were carried out in four traverse lines of the diffuser outlet transverse section (Fig. 2).

Altogether, there were 61 measurement locations/experimental points on each outlet traverse line. These points were not equidistant on the traverse line, but symmetric around the longitudinal axis of the diffuser. Table 1 shows the distances between the individual measurement points on each traverse line. Particular measurement points were consecutively numbered from 0 (diffuser wall) to 30 (longitudinal axis) on the traverse lines.

The aforementioned LDA system was used for visualization purposes as well. Namely, one of the beams of the LDA system having 514.5 nm wavelength was directed through a glass cylinder to form an illumination plane. The latter was positioned perpendicular to the diffuser's longitudinal axis at the diffuser outlet transverse section. Images of the diffuser outlet transverse section were taken with an analogous video camera, Sony video Hi8, type CCD TR820E, with a frequency of collecting the sequence of images f_s = 25 Hz. Images were digitised using the FAST AV Master Video Frame Grabber. The RAD Video Tools incl. Bink and Smacker

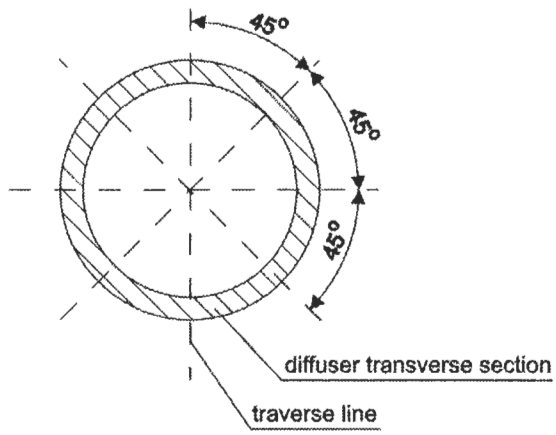

Fig. 2 Traverse lines in the diffuser outlet transverse section.

Table 1 Distances between Experimental Points on Each Traverse Line from the Diffuser Wall to Its Longitudinal Axis

Distance between individual experimental points (mm)	Consecuitive numbers of experimental points on the traverse lines at the diffuser outlet
0.5	0 to 10
1	10 to 20
3	20 to 25
5	25 to 29
6.135	29 to 30

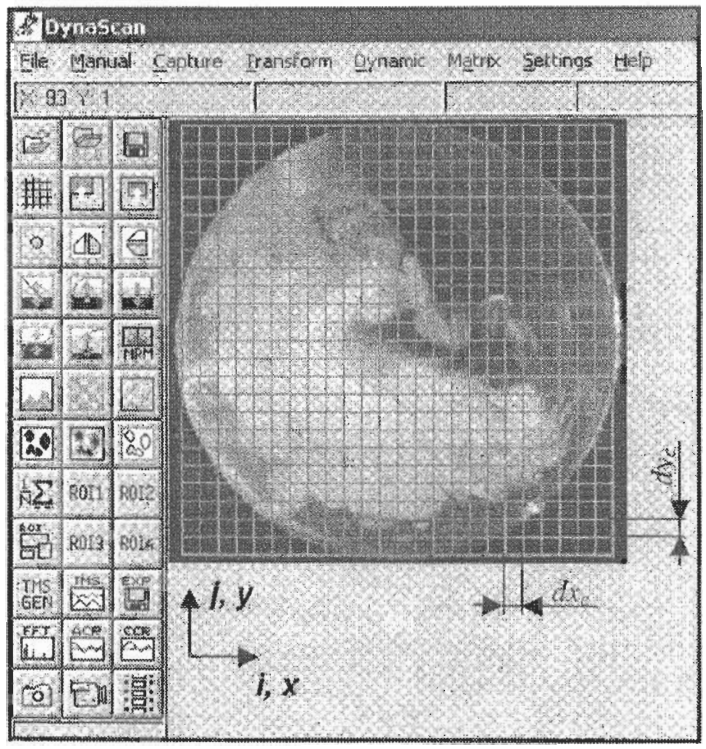

Fig. 3 Window with rectangular cells (placed above the diffuser outlet image).

program package enabled the transformation of the snapshot format from AVI to BMP. Sequences of images were then analysed through the Dynascan program package.

A window (ROI) was placed above each image of the diffuser outlet. This window was divided into a matrix $i \times j = 24 \times 24$ of equal cells as shown in Fig. 3. Each cell had a rectangular form of dimensions $dx_c \times dy_c = 10 \times 10$ pixels.

For every image in the sequence, an average grey level (A_c) in each window cell was calculated using the following formula [10]:

$$A_c(i,j,n) = \frac{1}{dy_c} \cdot \frac{1}{dx_c} \sum_{i_p=1}^{dy_c} \sum_{j_p=1}^{dx_c} E_p(i+i_p, j+j_p, n) \tag{2}$$

where $E_p(i + i_p, j + j_p)$ represents the grey intensity of the observed pixel at cell position (i, j) and relative position (i_p, j_p) of pixel within cell location; n denotes the consecutive number of an image in the sequence. The intensity of pixels $E_p(i + i_p, j + j_p)$ ranged from 0 (black) to 255 (white). The mean value of the grey intensity in each cell for the whole sequence of images is obtained from Eq. (3):

$$\mu_c(i,j) = \frac{1}{N} \sum_{n=1}^{N} A_c(i,j,n) \tag{3}$$

where N denotes the number of all images in the sequence; there were 100 images in each sequence. It can be seen from Fig. 3 that there is a sudden transition in grey levels from a low to a high value on the boundary of the main flow and the reverse flow. The former has high values of grey level because of the high concentration of pollutant droplets, whilst the latter has low values of grey level, as the reverse flow consists mainly of surrounding air, which contains virtually no pollutant droplets. The intensity of this grey level transition on the boundary between the two flows is described by a two-component gradient:

$$\nabla\mu(i,j) = \begin{bmatrix} \nabla\mu_i(i,j) \\ \nabla\mu_j(i,j) \end{bmatrix} = \begin{bmatrix} \dfrac{\partial\mu(i,j)}{\partial i} \\ \dfrac{\partial\mu(i,j)}{\partial j} \end{bmatrix} \tag{4}$$

where the scalar value (= norm) of Eq. (4) is:

$$\|\nabla\mu(i,j)\| = \sqrt{\left(\frac{\partial\mu(i,j)}{\partial i}\right)^2 + \left(\frac{\partial\mu(i,j)}{\partial j}\right)^2} \tag{5}$$

It was assumed that the maximum value of the grey level gradient took place at the main flow/reverse flow boundary. The position of the boundary was therefore determined by the position of the cell in each column i where the maximum value of the gradient appeared:

$$(i_m, j_m) = \max\left[\sqrt{\left(\frac{\partial \mu(i,j)}{\partial i}\right)^2 + \left(\frac{\partial \mu(i,j)}{\partial j}\right)^2}\right]_{i=const.} \qquad i = 1, 2, 24 \qquad (6)$$

i_m and j_m represent the co-ordinates of the cell with maximum grey-level gradient in each column i.

RESULTS

The distribution of the time-averaged mean values of velocity components at the diffuser outlet transverse section is presented through contour diagrams shaped by the Surfer Version 7 software pack. In fact, only one contour has been depicted — the zero-velocity line, which represents the boundary between the main flow and the reverse flow; the contour divides the diffuser outlet into hatched (main flow) and non-hatched (reverse flow) sections. All diagrams are presented in such a way as if one would look from the diffuser outlet in the direction of the diffuser inlet. The direction of rotation of the diffuser was anti-clockwise from this view.

The "Kriging" method applying a linear variogram model was chosen in diagrams in the case of LDA measurements. All measured values of the velocity component in the particular measuring points coincide with the diagram surface. Apart from the measuring points, a set of additional points was introduced in the diagrams as well. These points represented velocity component values lying between the measuring points in the diffuser outlet transverse section. They were obtained from the measured velocity component values using the linear interpolation method. This proved to be necessary in order to smooth the diagrams. For this purpose, 80 additional radial rays were introduced into the diffuser inlet and outlet transverse planes; they ran from the diffuser longitudinal axis to the diffuser wall. The angle between two adjacent rays was 4.5°. Each ray contained interpolated values of the velocity component at 51 equidistant points at the diffuser outlet transverse section.

Minimum Airflow

Figure 4a shows the results of the LDA method for determination of the zero-velocity line at a stationary diffuser outlet at minimum airflow ($\dot{V}$ = 4 l/s, Re_i = $5.84 \cdot 10^3$), while Fig. 4b depicts the zero-velocity line at the same operating conditions of the diffuser, obtained by the visualization method.

Comparison between Figs. 4a and b shows that the major part of the reverse flow occupies the right upper part in the diffuser outlet transverse section, as presented by both methods. There are, however, some differences between the results; it is obvious that the visualization method predicts larger amounts of reverse flow in

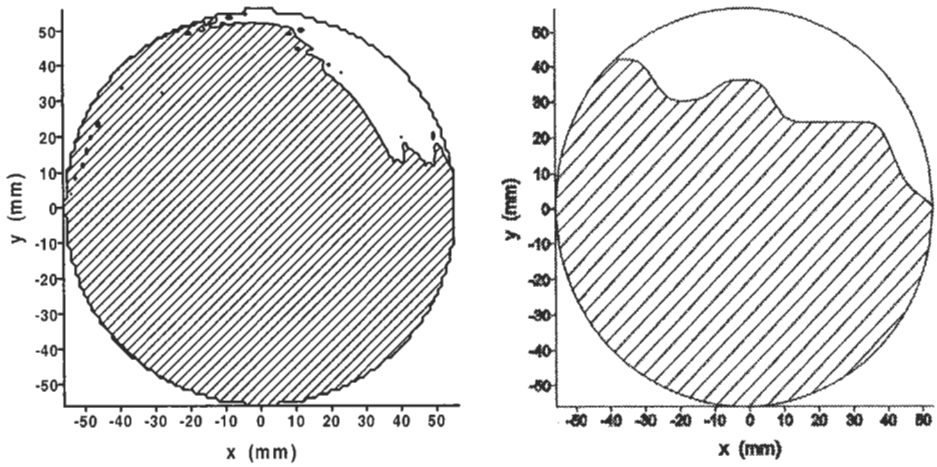

Fig. 4 Boundary between the main flow and the reverse flow in a stationary diffuser outlet at minimum applied airflow ($Re_i = 5.84 \cdot 10^3$). a) LDA method; b) visualization method.

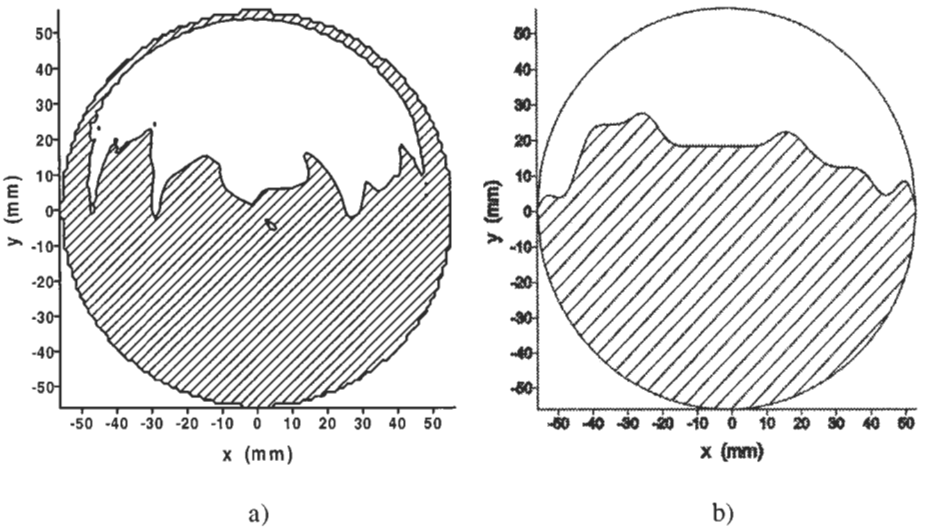

Fig. 5 Boundary between the main flow and the reverse flow in a rotating diffuser outlet at minimum applied airflow ($Re_i = 5.84 \cdot 10^3$). a) LDA method; b) visualization method.

comparison to the LDA method, since the area of the diffuser outlet transverse section occupied by the reverse flow is greater in Fig. 4b. Figure 5 shows the zero-velocity line in the outlet transverse section of a rotating diffuser.

Figure 5 shows that the region of the reverse flow is enlarged and its centre has moved in the direction of the diffuser rotation as compared to Fig. 4. It can be seen from Fig. 5 that the results of both methods are comparable, except for the thin boundary layer on the upper part of the diffuser outlet transverse section (Fig. 5a), which is not recognised by the visualization gradient method. This is the consequence of seeking just one maximum grey-level gradient value in each column i of the mesh shown in Fig. 3. But even when two maximum gradients were sought, the applied method would probably not find the near-wall outflow in the upper part of the diffuser, because this region is very thin (about 2–3-mm thick) and hardly observable even from the non-digitised images. This is also due to the fact that the illumination plane was positioned just outside the diffuser outlet (to avoid interference with the diffuser wall), so the majority of the flow in the upper thin layer had already turned in the radial direction when crossing the illumination plane.

The outflow in the near-wall region, as seen in Fig. 5a, is typical for rotating diffusers; it is related to the diffuser geometry and to the thickness of the diffuser wall at the diffuser outlet. The radial (centrifugal) force of airflow in a rotating diffuser is strongest at the wall and can be broken into two components: one component is perpendicular to the rotating diffuser wall and the other is parallel to it. Since the diffuser cone diverges in the direction of its outlet, one component of the centrifugal force is directed towards the diffuser outlet as well. The centrifugal force as the consequence of the rotating frequency thus results in substantial axial velocities in the near-wall (boundary layer) region (Fig. 5a).

The thickness of the wall at the diffuser outlet acts as an endplate. When the diffuser rotates, due to the centrifugal forces, the air attached to this endplate is pushed out of the diffuser in the radially-tangential direction [11]. Deficiency of air (and thereby pressure drop) at the inner radius of the endplate is compensated by the additional airflow sucked in by the endplate from the boundary layer inside the rotating diffuser cone. This is the second reason for the axial velocity peak in the near-wall region, and it is again dependent on the rotating frequency of the diffuser. Because of the above-described phenomena, flow separation from the rotating diffuser wall was never observed during the experiments, although the diffuser divergence angle exceeded 14°.

Comparison between Figs. 4 and 5 shows that the reverse flow region is not only much broader in the case of rotating diffuser, but also moved towards the longitudinal axis of the diffuser. This is clearly seen in Fig. 5. It is obvious that the vortex breakdown took place at the rotating diffuser outlet. A structural difference

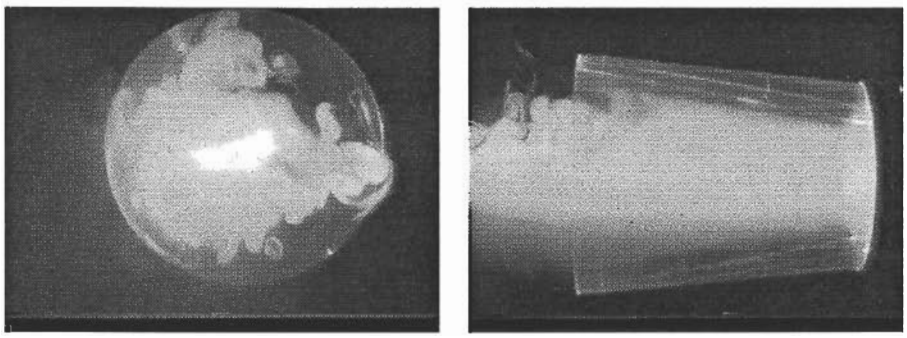

Fig. 6 Minimum applied airflow ($Re_i = 5.84 \cdot 10^3$) in a stationary diffuser.

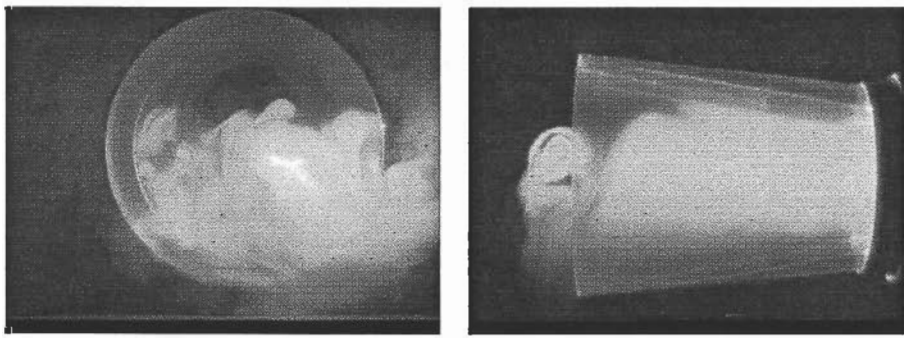

Fig. 7 Minimum applied airflow ($Re_i = 5.84 \cdot 10^3$) in a rotating diffuser.

between the airflow in a stationary diffuser with no vortex breakdown and a rotating diffuser where the vortex breakdown occurs is depicted in Figs. 6–7.

Higher Airflows

It is interesting that, when the airflow is higher, there is less area in the diffuser outlet transverse section occupied by the reverse flow. The core of the airflow is also more centrally aligned in the case of higher applied airflow $\dot{V}$= 8 l/s, $Re_i = 1.17 \cdot 10^4$), as shown in Figs. 8 and 9. This is almost certainly due to the Coanda effect [1], which is strongly felt in the case of minimum applied airflow ($Re_i = 5.84 \cdot 10^3$).

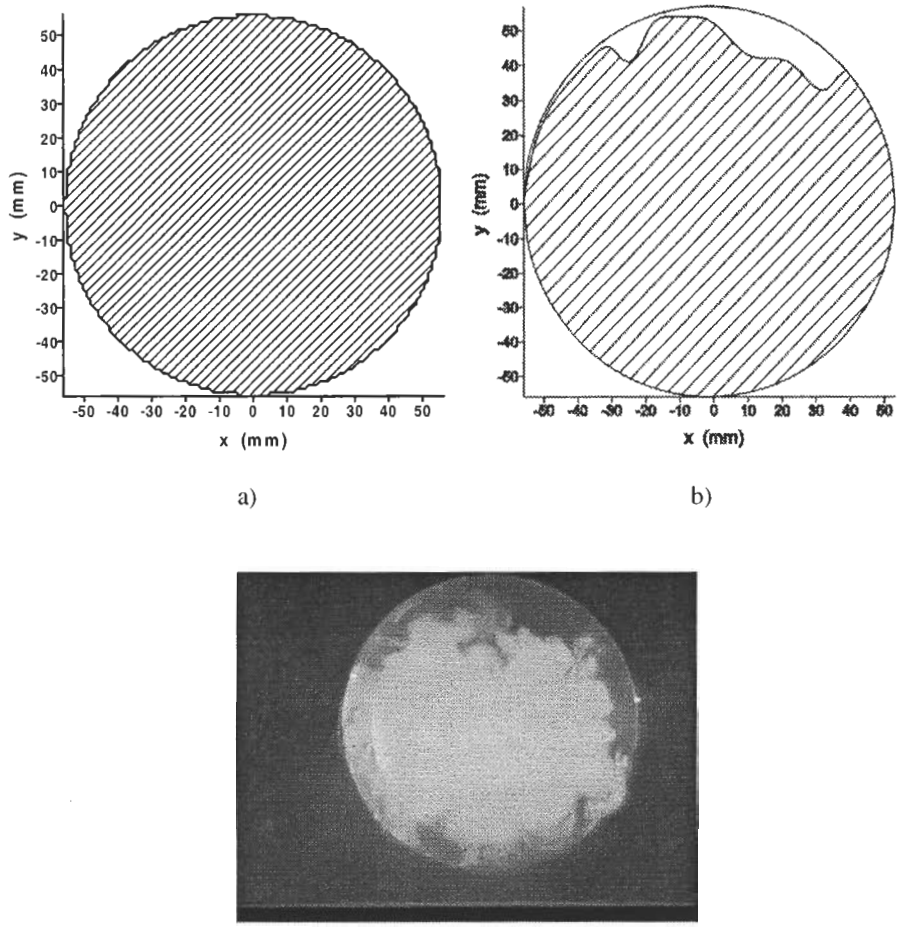

Fig. 8 Boundary between the main flow and the reverse flow in a stationary diffuser outlet at medium applied airflow ($Re_i = 1.17 \cdot 10^4$). a) LDA method; b) visualization method; c) image of the diffuser outlet.

The LDA method fails to predict the region of reverse flow in the outlet transverse section of a stationary diffuser with an airflow where $Re_i = 1.17 \cdot 10^4$ (Fig. 8a). This is the result of a very low data rate in the region of reverse flow (low concentration of pollutant droplets) and to the non-stationary nature of the airflow (main flow) core, which is due to the large divergence angle of the diffuser [1]; the region of reverse flow is therefore not always at the same place in the diffuser outlet trans-

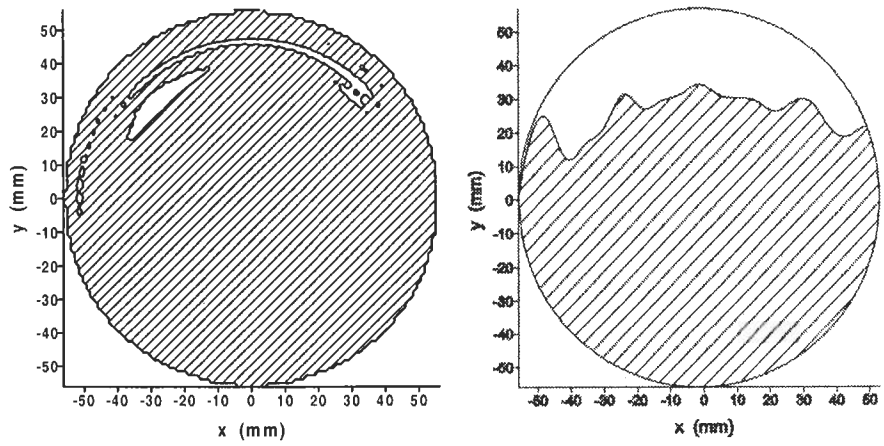

a) b)

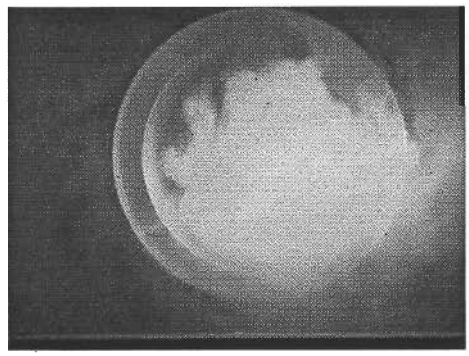

c)

Fig. 9 Boundary between the main flow and the reverse flow in a rotating diffuser outlet at medium applied airflow ($Re_i = 1.17 \cdot 10^4$). a) LDA method; b) visualization method; c) image of the diffuser outlet.

verse section, but changes its position slightly with time. The results of the visualization gradient method are thus closer to the real condition of the airflow at the diffuser outlet (Figs. 8b and c). On the other hand, the visualization gradient method cannot predict the thin near-wall outflow in the case of a rotating diffuser (Fig. 9b) — which is the result of the problems discussed in the previous section of the paper. The reverse flow region in the rotating diffuser outlet measured by the LDA

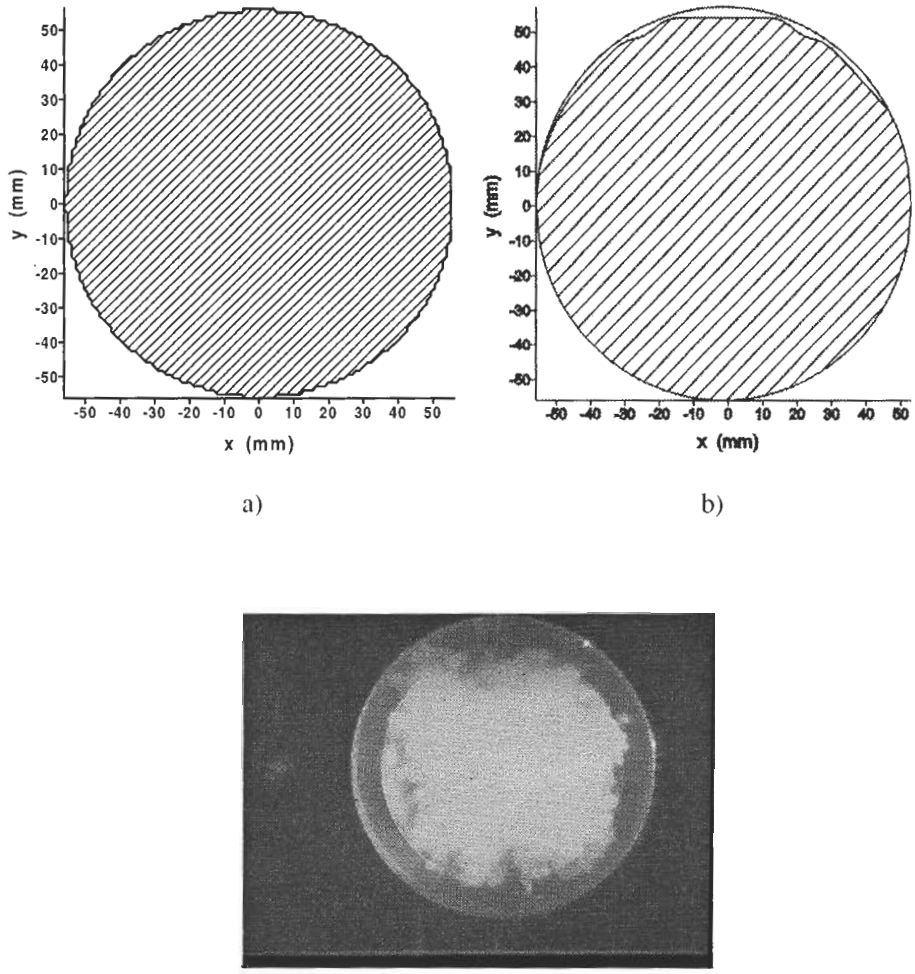

Fig. 10 Boundary between the main flow and the reverse flow in a stationary diffuser outlet at maximum applied airflow ($Re_i = 2.01 \cdot 10^4$). a) LDA method; b) visualization method; c) image of the diffuser outlet.

method is (in comparison with the stationary diffuser) again smaller than the real one (Figs. 9a and c). The slip of the centre of the recirculation zone in the direction

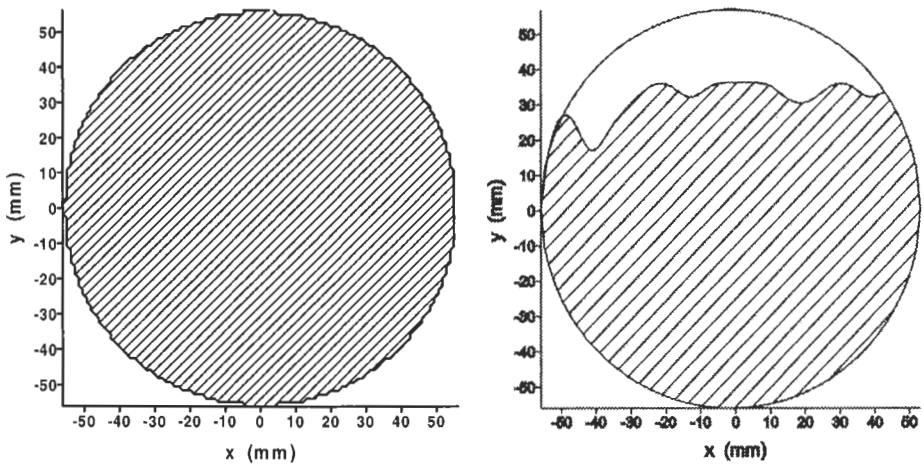

a) b)

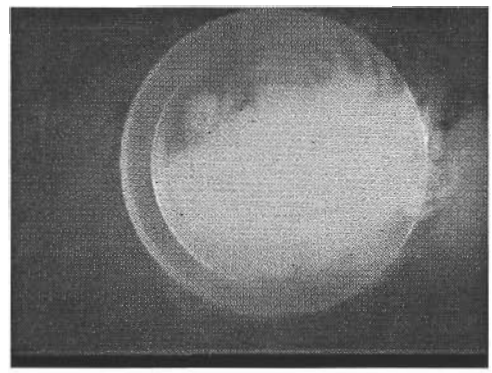

c)

Fig. 11 Boundary between the main flow and the reverse flow in a rotating diffuser outlet at maximum applied airflow ($Re_i = 2.01 \cdot 10^4$). a) LDA method; b) visualization method; c) image of the diffuser outlet.

of diffuser rotation is noticeable again (comparison between Figs. 8b and c and Figs. 9b and c).

Figures 10 and 11 depict the structure of airflow in the diffuser outlet transverse section in the case of maximum applied airflow ($\dot{V}$ = 13.8 l/s, $Re_i = 2.01 \cdot 10^4$).

There is not much difference in qualitative behaviour between medium and maximum applied airflows, as can be seen in Figs. 10 and 11. The reverse flow region was even smaller at the maximum applied airflow, and the results of the LDA method did not show it at all (Figs. 10a and 11a).

It is interesting that the reverse flow region was broader when the diffuser was rotating rather than being stationary, as shown in the images of the diffuser outlet. This happened not only in the case of the minimum airflow, but also at higher applied airflows, where no vortex breakdown occurred. This phenomenon is the result of asymmetrical airflow (with regard to the diffuser longitudinal axis) caused by recirculation zones. The airflow's asymmetry is thus enhanced when the diffuser rotates, because of the action of centrifugal force. Compared to the images of the diffuser outlet, the results of the visualization method are again generally better (i.e., closer to the state of airflow seen in the images of the diffuser outlet) than those obtained by the LDA method.

CONCLUSIONS

Two methods for detecting the reverse flow region in a stationary as well as rotating diffuser outlet were tested in the paper: the LDA method and the visualization method. The former method uses the principles of laser-Doppler anemometry and measures the airflow velocity components in each measuring (experimental) point. The boundary between the main flow and the reverse flow (zero axial velocity line) can thus be detected via the measured velocity field. The visualization method, however, deals with the airflow structure on the entire diffuser outlet transverse section at once. Here, the maximum grey-level gradient of polluted airflow represents the zero-velocity boundary.

The experiment revealed that the amount of volumetric flow and the rotating frequency significantly affect the shape and position of recirculation zones at the diffuser outlet. The area occupied by the reverse flow in the diffuser outlet transverse section increases if the diffuser rotates. On the other hand, an increasing amount of airflow (higher inlet Reynolds numbers) would shrink the area of recirculation in the outlet transverse section of the diffuser. It was also observed that the centre of the recirculation zone at the outlet transverse section of a stationary diffuser changed slightly its position (in the direction of rotation) as soon as the diffuser started to rotate.

A comparison between the two methods revealed their strengths and weaknesses. The results of the LDA method showed a reverse flow region which was

generally smaller than the one shown in the images of the diffuser outlet. The reason for such a deviation lies mainly in point-to-point measurements of velocity field in the unsteady (time-dependent) reverse flow. The LDA method could, however, find a reverse flow region which was encircled with a very thin region of outflow. On the other hand, the visualization method failed to find the boundary between the main flow and the reverse flow in cases where the main flow region was very thin. This is due to the small amount of pollutant in such a thin outflow region, and also to the calculation of only one maximum gradient in each column of cells when processing the images. But the results of the visualization method were generally very close to the actual situation, especially when considering the dimensions of the reverse flow region. It should be taken into account that the visualization method also uses averaging methods for finding the maximum gradient, but this is somewhat inevitable because of the (usually) unsteady nature of reverse flows.

It can be concluded that the visualization method could be quite successfully applied in searching for recirculation zones, since the cases with a thin outflow encircling the region of reverse flow (i.e., in the case of a rotating diffuser) are rare in practice. Recirculation zones are usually attached to the wall (i.e., in the case of a stationary diffuser) and are thus more suitable for qualitative analysis by the visualization method rather than by the LDA method. Naturally, the part of a pipe, channel, diffuser, etc. where the recirculation regions are searched for should be made of transparent material. If this is provided, and when the position and dimensions of the reverse flow region are in question, then the visualization method is quicker, simpler, generally more accurate, and also much cheaper in comparison with the LDA method.

REFERENCES

1. P. Bradshaw, *Turbulence, Topics in Applied Physics*, Springer-Verlag, Berlin, 1976.
2. A. Kovats, *Design and Performance of Centrifugal and Axial Flow Pumps and Compressors*, Pergamon Press Ltd., Oxford, 1964.
3. M. Murakami and K. Kikuyama, Turbulent Flow in Axially Rotating Pipes, *Journal of Fluids Engineering*, vol. 102, pp. 97–103, 1980.
4. S. Imao, M. Itoh, and T. Harada, Turbulent Characteristics of the Flow in an Axially Rotating Pipe, *Int. J. Heat and Fluid Flow*, vol. 17, no. 5, pp. 444–451, 1996.
5. A. K. Gupta, D. G. Lilley, and N. Syred, *Swirl Flows*, Abacus Press, Tunbridge Wells, 1984.

6. O. Lucca-Negro and T. O'Doherty, Vortex Breakdown: A Review, *Progress in Energy and Combustion Science*, vol. 27, pp. 431–481, 2001.
7. A. M. Mitchell and J. Delery, Research into Vortex Breakdown Control, *Progress in Aerospace Sciences*, vol. 37, pp. 385–418, 2001.
8. P. Billant, J.-M. Chomaz, and P. Huerre, Experimental Study of Vortex Breakdown in Swirling Jets, *J. Fluid Mech.*, vol. 376, pp. 183–219, 1998.
9. M. Goldshtik and F. Hussain, Analysis of Inviscid Vortex Breakdown in a Semi-infinite Pipe, *Fluid Dynamics Research*, vol. 23, pp. 189–234, 1998.
10. F. Trdic, B. Sirok, P. R. Bullen, and D. R. Philpott, Monitoring Mineral Wool Production Using Real-time Machine Vision, *Real-time Imaging*, vol. 5, no. 2, pp. 125–140, 1999.
11. H. Schlichting and K. Gersten, *Boundary-Layer Theory*, Springer, Berlin, 2000.